Title	Photostimulation induced persistent luminescence in $Y_3Al_2Ga_3O_{12}:Cr^{3}$
Author(s)	Katayama, Yumiko; Viana, Bruno; Gourier, Didier; Xu, Jian; Tanabe, Setsuhisa
Citation	Optical Materials Express (2016), 6(4): 1405-1413
Issue Date	2016-04-01
URL	http://hdl.handle.net/2433/231978
Right	© 2016 Optical Society of America]. Users may use, reuse, and build upon the article, or use the article for text or data mining, so long as such uses are for non-commercial purposes and appropriate attribution is maintained. All other rights are reserved.
Type	Journal Article
Textversion	publisher

Photostimulation induced persistent luminescence in $Y_3Al_2Ga_3O_{12}:Cr^{3+}$

Yumiko Katayama,[1,*] Bruno Viana,[2] Didier Gourier,[2] Jian Xu,[1] and Setsuhisa Tanabe[1]

[1]*Graduate School of Human and Environmental Studies, Kyoto University, 606-8501 Kyoto, Japan*
[2]*PSL Research University, Chimie ParisTech – CNRS, Institut de Recherche de Chimie Paris, 75005 Paris, France*
**katayama.yumiko.48a@st.kyoto-u.ac.jp*

Abstract: Cr^{3+}-activated $Y_3Al_2Ga_3O_{12}$ garnet (YAG*G*:Cr^{3+}) persistent phosphor has been recently reported as a potential candidate material for *in vivo* imaging application. Temperature dependence of photoluminescence (PL) spectra and thermostimulated luminescence (TSL) glow curves with several conditions, especially photostimulation wavelength dependence, were carefully investigated with the perspective of deep trap utilization for long-term *in vivo* imaging. The PL spectrum showed typical Cr^{3+} emission due to $^2E \rightarrow {}^4A_2$ and $^4T_2 \rightarrow {}^4A_2$ transitions. The integrated PL intensity of Cr^{3+} luminescence ($^2E \rightarrow {}^4A_2$ plus $^4T_2 \rightarrow {}^4A_2$ transitions) does not suffer from temperature quenching up to 600 K. From the TSL glow curve measurements, it was found that the persistent luminescence cannot be activated by visible light excitation. However, photostimulation induced persistent luminescence by red to near-infrared light can be possible in this material.

OCIS codes: (160.2540) Fluorescent and luminescent materials; (090.2900) Optical storage materials; (160.6990) Transition-metal-doped materials; (170.3880) Medical and biological imaging.

References and links

1. T. Matsuzawa, Y. Aoki, N. Takeuchi, and Y. Murayama, "A new long phosphorescent phosphor with high brightness, $SrAl_2O_4:Eu^{2+},Dy^{3+}$," J. Electrochem. Soc. **143**(8), 2670–2673 (1996).
2. G. Portal, "Review of the principal materials available for thermoluminescent dosimetry," Radiat. Prot. Dosimetry **17**, 351–357 (1986).
3. K. Takahashi, J. Miyahara, and Y. Shibahara, "Photostimulated luminescence (PSL) and color centers in $BaFX:Eu^{2+}$ (X = Cl, Br, I) phosphors," J. Electrochem. Soc. **132**(6), 1492–1494 (1985).
4. Q. le Masne de Chermont, C. Chanéac, J. Seguin, F. Pellé, S. Maîtrejean, J.-P. Jolivet, D. Gourier, M. Bessodes, and D. Scherman, "Nanoprobes with near-infrared persistent luminescence for in vivo imaging," Proc. Natl. Acad. Sci. U.S.A. **104**(22), 9266–9271 (2007).
5. A. Lecointre, A. Bessière, B. Viana, and D. Gourier, "Red persistent luminescent silicate nanoparticles," Radiat. Meas. **45**(3-6), 497–499 (2010).
6. A. Bessière, S. Jacquart, K. Priolkar, A. Lecointre, B. Viana, and D. Gourier, "$ZnGa_2O_4:Cr^{3+}$: a new red long-lasting phosphor with high brightness," Opt. Express **19**(11), 10131–10137 (2011).
7. T. Maldiney, G. Sraiki, B. Viana, D. Gourier, C. Richard, D. Scherman, M. Bessodes, K. Van den Eeckhout, D. Poleman, and P. F. Smet, "In vivo optical imaging with rare earth doped $Ca_2Si_2N_8$ persistent luminescence nanoparticles," Opt. Mater. Express **2**(3), 261–268 (2012).
8. Y. Katayama, J. Ueda, and S. Tanabe, "Effect of Bi_2O_3 doping on persistent luminescence of $MgGeO_3:Mn^{2+}$ phosphor," Opt. Mater. Express **4**(4), 613–623 (2014).
9. Y. Zhuang, Y. Katayama, J. Ueda, and S. Tanabe, "A brief review on red to near-infrared persistent luminescence in transition-metal-activated phosphors," Opt. Mater. **36**(11), 1907–1912 (2014).
10. J. Xu, J. Ueda, Y. Zhuang, B. Viana, and S. Tanabe, "$Y_3Al_{5-x}Ga_xO_{12}:Cr^{3+}$: A novel red persistent phosphor with high brightness," Appl. Phys. Express **8**(4), 042602 (2015).
11. R. Weissleder, "A clearer vision for in vivo imaging," Nat. Biotechnol. **19**(4), 316–317 (2001).
12. T. Maldiney, A. Bessière, J. Seguin, E. Teston, S. K. Sharma, B. Viana, A. J. J. Bos, P. Dorenbos, M. Bessodes, D. Gourier, D. Scherman, and C. Richard, "The in vivo activation of persistent nanophosphors for optical imaging of vascularization, tumours and grafted cells," Nat. Mater. **13**(4), 418–426 (2014).
13. F. Liu, Y. Liang, and Z. Pan, "Detection of up-converted persistent luminescence in the near infrared emitted by the $Zn_3Ga_2GeO_8:Cr^{3+}$, Yb^{3+}, Er^{3+} phosphor," Phys. Rev. Lett. **113**(17), 177401 (2014).

#256933 Received 8 Jan 2016; revised 7 Mar 2016; accepted 8 Mar 2016; published 31 Mar 2016

14. A. Bessière, S. K. Sharma, N. Basavaraju, K. R. Priolkar, L. Binet, B. Viana, A. J. J. Bos, T. Maldiney, C. Richard, D. Scherman, and D. Gourier, "Storage of visible light for long-lasting phosphorescence in chromium-doped zinc gallate," Chem. Mater. **26**(3), 1365–1373 (2014).
15. Y. Zhuang, J. Ueda, and S. Tanabe, "Tunable trap depth in $Zn(Ga,Al)_2O_4$ Cr, Bi red persistent phosphors considerations of high temperature persistent luminescence and photostimulated persistent luminesence," J. Mater. Chem. C Mater. Opt. Electron. Devices **1**(47), 7849–7855 (2013).
16. F. Liu, W. Yan, Y.-J. Chuang, Z. Zhen, J. Xie, and Z. Pan, "Photostimulated near-infrared persistent luminescence as a new optical read-out from Cr^{3+}-doped $LiGa_5O_8$," Sci. Rep. **3**, 1554 (2013).
17. D. C. Rodríguez Burbano, S. K. Sharma, P. Dorenbos, B. Viana, and J. A. Capobianco, "Persistent and Photostimulated Red Emission in $CaS:Eu^{2+},Dy^{3+}$ Nanophosphors," Adv. Opt. Mater. **3**(4), 551–557 (2015).
18. J. Xu, J. Ueda, K. Kuroishi, and S. Tanabe, "Fabrication of Ce^{3+}–Cr^{3+} co-doped yttrium aluminium gallium garnet transparent ceramic phosphors with super long persistent luminescence," Scr. Mater. **102**, 47–50 (2015).
19. P. Dorenbos, "Electronic structure and optical properties of the lanthanide activated $RE_3(Al_{1-x}Ga_x)_5O_{12}$ (RE=Gd, Y, Lu) garnet compounds," J. Lumin. **134**, 310–318 (2013).
20. J. P. Hehir, M. O. Henry, J. P. Larkin, and G. F. Imbusch, "Nature of the luminescence from $YAG:Cr^{3+}$," J. Phys. C Solid State Phys. **7**(12), 2241–2248 (1974).
21. M. Yamaga, B. Henderson, K. P. O'Donnell, and G. Yue, "Temperature dependence of the lifetime of Cr^{3+} luminescence in garnet crystals II. The case of YGG," Appl. Phys. B **51**, 132–136 (1990).
22. B. Henderson, A. Marshall, M. Yamaga, K. P. O'Donnell, and B. Cockayne, "The temperature dependence of Cr^{3+} photoluminescence in some garnet crystals," J. Phys. C Solid State Phys. **21**(36), 6187–6198 (1988).
23. W. A. Wall, J. T. Karpick, and B. Di Bartolo, "Temperature dependence of the vibronic spectrum and fluorescence lifetime of $YAG:Cr^{3+}$," J. Phys. C Solid State Phys. **4**(18), 3258–3264 (1971).
24. P. Avouris and T. N. Morgan, "A tunneling model for the decay of luminescence in inorganic phosphors: The case of Zn_2SiO_4:Mn," J. Chem. Phys. **74**(8), 4347–4355 (1981).
25. A. Dobrowolska, A. J. J. Bos, and P. Dorenbos, "Electron tunnelling phenomena in YPO_4 : Ce,Ln (Ln = Er, Ho, Nd, Dy)," J. Phys. D Appl. Phys. **47**(33), 335301 (2014).
26. S. W. S. McKeever, *Thermoluminescence of Solids*, Cambridge Solid State Science Series (Cambridge University Press, Cambridge, 1988), p. 392.
27. K. Van den Eeckhout, A. J. J. Bos, D. Poelman, and P. Smet, "Revealing trap depth distributions in persistent phosphors," Phys. Rev. B **87**(4), 045126 (2013).

1. Introduction

Persistent phosphors are materials that show delayed luminescence after stopping excitation light. The delay originates from carrier trapping defects in the forbidden bandgap of materials, which are generated in most cases by irradiation with X-ray or ultraviolet (UV) light, and in rare cases by visible light excitation. Persistent luminescence is observed when the trap depths of these defects are sufficiently small to permit charge release by ambient thermal energy. On the other hand, materials that have deeper traps are called storage phosphor. The stored carriers are released by additional thermal- or photostimulation, which results in thermally stimulated luminescence (TSL) and photo-stimulated luminescence (PSL), respectively. TSL glow curve measurement that records TSL intensity against temperature with constant heating rate is one of the most important techniques to gain information on the trap depths and distributions in the material. Good persistent phosphors such as $SrAl_2O_4:Eu^{2+}$-Dy^{3+} show a TSL peak in the range from 250 K to 350 K [1].

Persistent and storage phosphors have been developed for wide range of applications such as night lightning, safety signs, dosimeters, infrared light checkers, *in vivo* imaging and so on [1–4]. Especially for *in vivo* optical imaging of small animals, several red to near infrared (NIR) persistent phosphors have been reported [5–10] because biological tissues have higher transmittance in this range, i.e. between 600 and 1100 nm (biological window) [11]. In 2007, Le Masne de Chermont *et. al.* reported first demonstration of *in vivo* imaging of mouse using Mn^{2+} activated persistent luminescent nano particles [4]. Comparing with other biomarkers using excitation light during imaging, UV excitation before injection can lead to higher signal to noise ratio due to the absence of autofluorescence from animal tissues [12]. However, in case of persistent phosphors that can be activated only by UV light, the detecting time is limited because persistent luminescence decays with time and UV excitation cannot be repeated owing to the lack of transparency of living tissues in the UV. For the long-term *in vivo* imaging, additional characteristics, such as upconversion [13], red excitable persistent luminescence [14], PSL under NIR photostimulation [15–17], and photostimulation induced persistent luminescence [16] have been reported.

#256933 Received 8 Jan 2016; revised 7 Mar 2016; accepted 8 Mar 2016; published 31 Mar 2016

Recently, Cr^{3+}-activated $Y_3Al_2Ga_3O_{12}$ garnet (YAG*G*:Cr^{3+}) persistent phosphor has been reported as a promising candidate material for *in vivo* imaging application [10]. The YAG*G*:Cr^{3+} is already known to show strong persistent luminescence peaking at 690 nm due to $^2E \rightarrow {}^4A_2$ transition of Cr^{3+} after ceasing UV excitation. The persistent luminescence intensity after UV excitation is even stronger (in radiance unit) than the well-studied red-NIR persistent phosphor, $ZnGa_2O_4$:Cr^{3+}. In addition, YAG*G*:Cr^{3+} is both persistent phosphor and photo-storage phosphor because it shows two strong TSL glow peaks approximately at 300 K and 400 K. The TSL peak at 400 K is stable at ambient temperature whereas the peak at 300 K is active for persistent luminescence. Therefore, the deeper traps in YAG*G*:Cr^{3+} can also be utilized for additional detection for *in vivo* imaging application.

In this paper, taking advantage of the features of YAG*G*:Cr^{3+}, effects of photostimulation on TSL glow curves of YAG*G*:Cr^{3+} were studied as well as temperature dependence of PL and excitation wavelength dependence of TSL glow curve. We report that YAG*G*:Cr^{3+} shows PSL and the photostimulation induced persistent luminescence by red light photostimulation.

2. Experimental

2.1 Sample preparation

Cr^{3+} doped YAG*G* phosphor with a composition of $Y_3Al_{1.99}$ $Cr_{0.01}Ga_3O_{12}$ was prepared by solid state reaction method. Y_2O_3(99.99%), Al_2O_3(99.99%), Ga_2O_3(99.99%) and Cr_2O_3(99.9%) were used as raw materials. The starting powder was mixed by ball milling (Fritsch Premium Line P-7) with Al_2O_3 ceramic balls and anhydrous ethanol. After drying, the mixed powder was compacted to form a ceramic green body with 20-mm-diameter under uniaxial pressing of 50 MPa, and finally sintered at 1600 °C for 10 h in vacuum. This results to translucent pellets as seen for instance in ref [18].

2.2 Photoluminescence and thermally stimulated luminescence glow curves

For TSL glow curve measurement, powder sample was fixed with a silver glue on the cold finger of a closed cycle helium cryogenerator. TSL was recorded by the same detector as PL measurement after 5 min excitation with heating rate of 10 K/min. TSL glow curves were obtained by integrating TSL spectra in the range from 597 nm to 896 nm. Excitation light sources in the UV (254 nm) was produced by a 6W Hg fluorescent tube (VILBER LOURMAT VL-6C) and excitations in blue and red were produced by LEDs peaking at 455 nm and 625 nm (Thorlab M625L3) were used. Photostimulation was induced by the red LED and by NIR laser diodes at 808 nm and 976 nm (LIMO3-F200-DL808, LIMO7-F200-DL976), with output power of 500 mW and 2000 mW, respectively. The output power of the red LED is ~700 mW with input current 1000 mA. Note that the absolute powers of the incident light cannot be compared because both output power and divergence angle of the light sources are different. Different time and temperature cycle were used in order to reveal persistent luminescence, and PSL ability of the material. Photostimulation-induced persistent luminescence decay curve was recorded at 300 K after 5 min UV excitation, 2 h initial decay and 1 min red photostimulation.

Temperature dependence of PL spectra under 455nm blue excitation (Thorlab M455L2) was recorded with the same set up as TSL glow curve measurement. The recorded PL spectra were corrected for the detector response using a standard halogen lamp (AVANTES AvaLight-HAL-CAL-ISP). Photoluminescence excitation (PLE) spectra monitoring Cr^{3+} luminescence at room temperature was recorded by a fluorescence spectrophotometer (Agilent Cary-Eclipse).

3. Results and discussions

3.1 Photoluminescence properties

Figure 1 shows the PL and PLE spectra of the YAG*G*:Cr^{3+} phosphor. The PL spectrum shows a sharp luminescence line of Cr^{3+} peaking at 689 nm due to $^2E \rightarrow {}^4A_2$ zero-phonon transition

#256933 Received 8 Jan 2016; revised 7 Mar 2016; accepted 8 Mar 2016; published 31 Mar 2016

(*R*-line) with some phonon sidebands and a broad luminescence band due to $^4T_2 \rightarrow {}^4A_2$ transition peaking approximately at 720 nm. In the PLE spectrum, three PLE bands peaking at 619 nm, 447 nm and 284 nm were observed and these bands were attributed to $^4A_2 \rightarrow {}^4T_2(^4F)$, $^4A_2 \rightarrow {}^4T_1(^4F)$ and $^4A_2 \rightarrow {}^4T_1(^4P)$, respectively. Bandgap energy E_g in this material is 7.02 eV [19]. PL and PLE spectra are consistent with those reported in literatures [10, 20, 21]. Strong persistent luminescence due to Cr^{3+} transitions was also observed after 254 nm excitation, and the persistent luminescence spectrum was the same as the PL spectrum. Thus, the persistent luminescence occurs through the same type of Cr^{3+} centers as the PL.

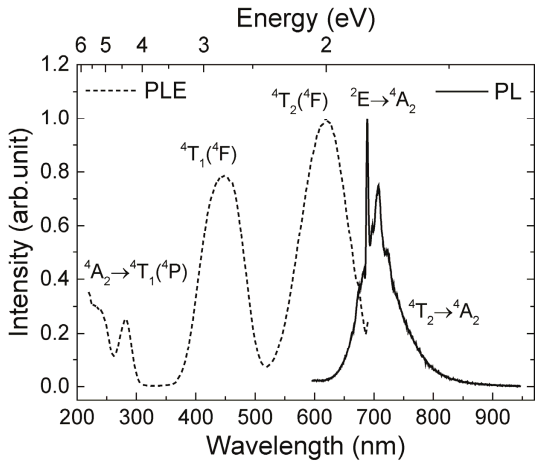

Fig. 1. PLE spectrum monitoring at 690 nm and PL spectrum under 455 nm excitation of the YAG*G*:Cr^{3+} at room temperature.

From application point of view, it is important to know the temperature dependence of the total PL intensity of $^2E \rightarrow {}^4A_2$ and $^4T_2 \rightarrow {}^4A_2$ emission bands. Figure 2 shows the temperature dependence of PL spectra under 455 nm excitation in the range from 10 K to 600 K. Inserted figure shows corresponding integrated intensity of Cr^{3+} luminescence. The shapes of the PL spectra changed a lot during heating. At low temperature, a sharp *R*-line luminescence peak was observed with some stokes phonon sidebands. With increasing temperature, a broad luminescence band due to $^4T_2 \rightarrow {}^4A_2$ transition appears and the *R*-line peak could not be observed when the temperature reached 600 K. The integrated PL intensity in the range from 597 nm to 896 nm increased with increasing temperature from 100 K to 500 K and decreased above 500 K.

Temperature dependent change in PL spectra is due to thermal expansion of lattice during heating, which results in weaker crystal field of Cr^{3+} ions. Similar changes in the PL spectrum have been reported in garnet structures such as Cr^{3+} activated YA*G* and YG*G* [21–23]. Though we have no clear explanation for the slight increase in the 100 K to 500 K temperature range, there are thermal quenching of the spin forbidden $^2E \rightarrow {}^4A_2$ *R*-line which is compensated by the increase of emission from the $^4T_2$ level. The weak decrease above 500 K is due to a thermal quenching from $^4T_2$ to $^4A_2$ ground state.

From these results, YAG*G*:Cr^{3+} is found to be a good phosphor with quite low thermal quenching. Therefore, the following TSL glow curves were not necessarily corrected by temperature dependence of the PL intensity.

#256933 Received 8 Jan 2016; revised 7 Mar 2016; accepted 8 Mar 2016; published 31 Mar 2016

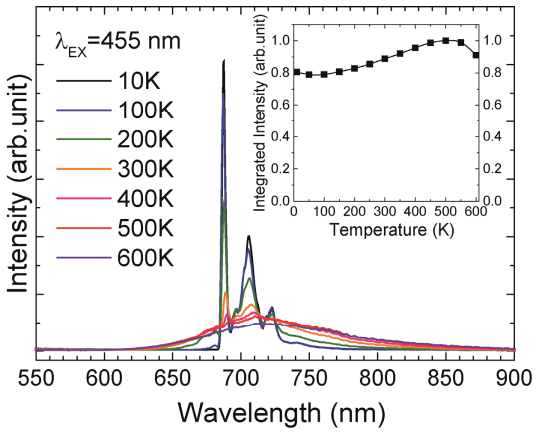

Fig. 2. Temperature dependence of PL spectra at different temperatures from 10 K to 600 K. Inserted figure shows integrated PL intensity in the range from 597 nm to 896 nm.

3.2 Thermoluminescence properties

3.2.1 Excitation wavelength dependence

Figure 3 shows the TSL glow curves recorded after 254 nm, 455 nm and 625 nm excitations. Note that the glow curves after visible excitations are multiplied by 80 from the raw data. After 254 nm UV excitation, the TSL glow curve shows two peaks, Peak (I) with peak temperature T_m = 311 K and Peak (II) with T_m = 394 K, which are almost the same temperature reported before [10]. In addition to these two bands, TSL intensity is also clearly observed below 200 K. This background TSL was not observed when the TSL glow curve was measured after 1 h-waiting at 10 K before heating. These results are indicative of radiative recombination by athermal tunneling from trapping centers nearby Cr^{3+} in this material [24–26].

Let us now consider the results after visible excitations. It should be noted that in case of visible light excitations, low temperature decay below 100 K is due to change in dark current of the Si CCD detector, and rises in high temperature above 500 K are due to the increase of black body radiation in NIR range. After 455 nm blue excitation, the TSL intensity is much weaker than that after 254 nm excitation and glow curve shows only one peak at 435 K, which is at higher temperature than Peak (II). No TSL peak was observed after red light excitation.

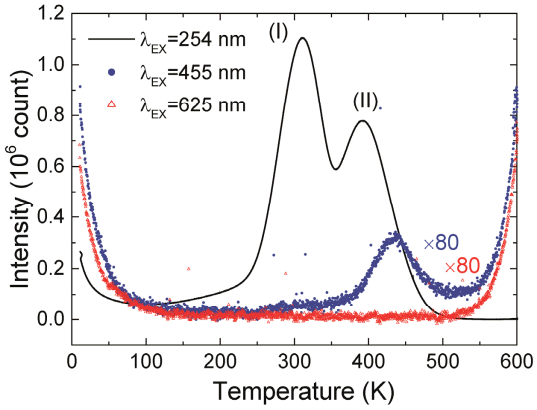

Fig. 3. TSL glow curves after different wavelength excitations, 254 nm, 455 nm and 625 nm. All glow curves measured just after stopping excitation light.

#256933 Received 8 Jan 2016; revised 7 Mar 2016; accepted 8 Mar 2016; published 31 Mar 2016

The effective trap generation under UV excitation is most probably due to the charging through the conduction band. Alternatively, TSL signal after blue excitation was weak and only part of Peak (II) (deeper traps) was created. This result suggests that charging from Cr^{3+} under blue light excitation is not effective through the conduction band. In other words, trap generation could only occur nearby Cr^{3+}. The shift in the position of the main peak maximum indicates the presence of distribution of trap depths in the material. Red light excitation energy do not give access to these traps, contrary to the case of $ZnGa_2O_4:Cr^{3+}$ material [14].

The trap depth energy E_{trap}, Peak (I) and Peak (II) are listed in Table 1. E_{trap} was estimated by using initial rise method [26]. It is first important to remove the effects of the athermal radiative recombinations and of the shallow traps (T<200 K). This was done by thermal cleaning at 200 K for Peak (I). Same procedure was used for Peak (II) at 300 K. The E_{trap} values measured by initial rise method were found to be 0.38 eV and 0.76 eV for Peak (I) and (II), respectively. These values represent shallowest trap depth of each kind of traps. This confirmed that the traps corresponding to Peak (II) are indeed deeper than that of Peak (I) but of course, distribution of trap depths are likely to occur for these two peaks as reported in literature [27].

Table 1. TSL glow peak temperature, T_m (K) and trap depth E_{trap} (eV) estimated by initial rise method. (I) and (II) represent peaks observed in classical TSL measurement. (i), (ii) and (iii) are trap depths measured after (i) 1.98 eV, (ii) 1.53eV and (iii) 1.27eV photostimulation induced after detrapping the shallower traps at ambient temperature.

	I	II		See Fig. 3
T_m (K)	311	394		
E_{trap} (eV)	0.38	0.76		
	i	ii	iii	See Fig. 6
T_m (K)	331	-	-	
E_{trap} (eV)	0.42	0.48	0.51	

3.2.2 Photostimulation effect on TSL glow curve

Figure 4 shows the TSL glow curves after 254 nm excitations with two waiting times and temperatures, 10 K for 1 h (Dashed curve) and 300 K for 2 h (Solid curve). This result clearly shows that the shallower traps (Peak (I)) plays a role for persistent luminescence and the deeper traps (Peak (II)) are still remaining 2 h after excitation at 300 K. To investigate the photostimulation effects on TSL glow curves, two kinds of measurements were performed. One is TSL glow curve measurement after PSL; TSL glow curves were measured after 254 nm excitation for 5 min with subsequent photostimulation for 1 h by several excitation wavelength. Both excitation and photostimulation were performed at 10 K. The other was measured to evaluate photo-transfer phenomenon. Photo-transfer is electron trapped at deeper trap photo-ionized and retrapped at shallower trap, which is key trap for persistent luminescence.

PSL is one of the ways to obtain signals from storage phosphors. Figure 5 shows a set of TSL glow curves recorded when the samples excited at 254 nm were additionally photostimulated for 1 h by 977 nm (1.27 eV), 808 nm (1.53 eV) and 625 nm (1.98 eV) light sources. A waiting time of 1 h was applied between the 254 nm excitation and the photostimulation. Excitation, photostimulation and waiting were done at 10 K. The lower panel of Fig. 5 shows the normalized differences between each photostimulated TSL curves and the TSL curve without photostimulation. By 977 nm and 808 nm photostimulations, significant decrease of Peak (I) was observed whereas Peak (II) only weakly decreased. On the other hand, by 625 nm red excitation (1.98 eV), both Peak (I) and Peak (II) strongly decreased. The difference curve from original TSL curves show peak shift to the higher temperature with increasing photostimulation photon energy.

In case of YAG*G*:Cr^{3+}, stimulations at 977 nm and 808 nm are not sufficient to detrap the deeper traps and red light stimulation at 625 nm is required to get PSL.

#256933 Received 8 Jan 2016; revised 7 Mar 2016; accepted 8 Mar 2016; published 31 Mar 2016

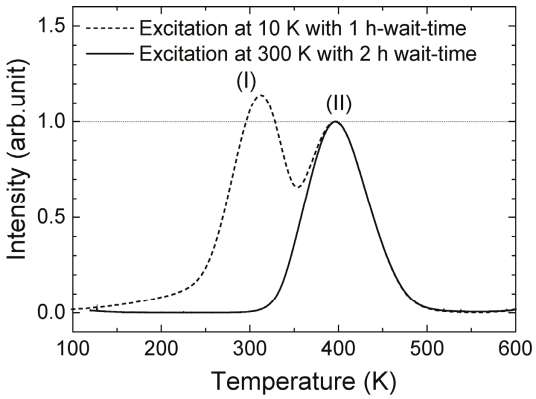

Fig. 4. TSL glow curves after 254 nm excitations for 5 min with different waiting time and temperature, excitation at 10 K with 1 h wait-time (Dashed curve) and excitation at 300 K with 2 h wait-time (Solid curve).

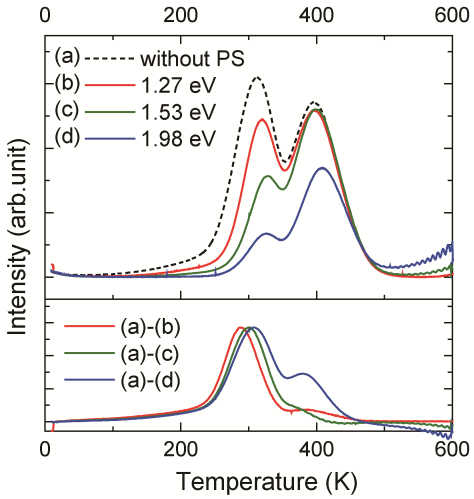

Fig. 5. TSL glow curve measured 1 h after 254 nm excitation for 5 min at 10 K (a) and TSL glow curves measured after 254 nm excitation for 5 min and subsequent photostimulation at 10 K for 1 h by (b)977 nm (1.27 eV), (c) 808 nm(1.53 eV) and (d) 625 nm (1.98 eV) (upper figure) excitations. Curves in lower figure are each subtraction curves from the curve (a), normalized with respect to the difference measured for peak (I) intensity.

Figure 6(a) shows photostimulation photon energy dependence on TSL glow curve after detrapping the shallower traps (I) at ambient temperature for 1 h. After 254 nm excitation for 5 min at 300 K, sample temperature was kept at 300 K for 2 h to remove the shallower trap (I), then cooled down to 120 K, and kept 1 h at this temperature for waiting (this is the TSL curve shown in Fig. 4 as solid curve) or photostimulation before heating. With increasing photostimulation energy from 1.27 to 1.98 eV, one observed the increase of the TSL intensity in a part of Peak (I) at around 330 K and peak (II) shifts to higher temperature. This tendency was efficient with higher photon energy photostimulation. This result strongly indicates that persistent luminescence can be reactivated by red (1.53 eV and 1.98 eV photons) photostimulation. The shallowest trap depth induced by the photostimulation was estimated by applying initial rise method to the TSL curves (i), (ii) and (iii) (Fig. 6(b), Table 1). Significant change in trap depth was observed even after 1.27 eV photostimulation. The estimated trap depths were 0.51 eV for 977 nm, 0.48 eV for 808 nm and 0.42 eV for 625 nm photostimulation, clearly revealing the traps distribution.

#256933 Received 8 Jan 2016; revised 7 Mar 2016; accepted 8 Mar 2016; published 31 Mar 2016

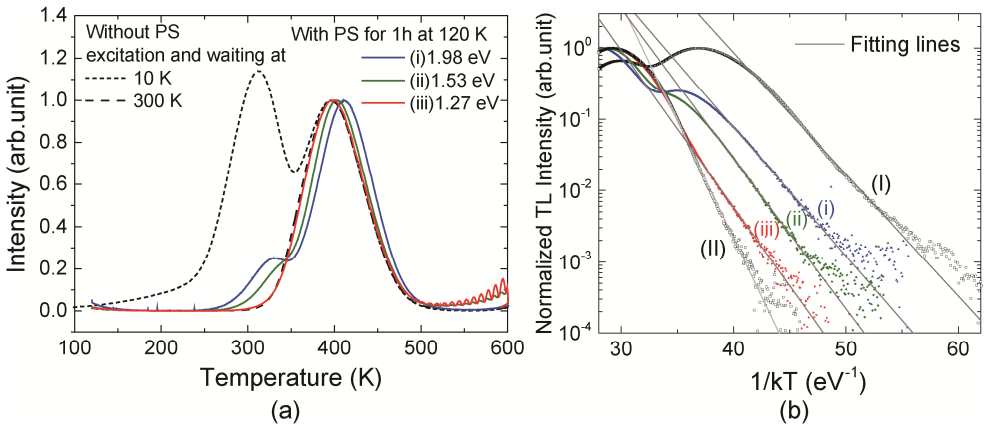

Fig. 6. Photostimulation photon energy dependence on TSL glow curves after detrapping the shallower traps in YAG*G*:Cr^{3+}. After 254 nm excitation for 5 min at 300 K, sample temperature was kept at 300 K for 2 h, then cooled down to 120 K, and kept 1 h at this temperature for waiting or photostimulation before heating. The TSL glow curves in Fig. 5 are plotted as references.

3.3 Mechanism of persistent luminescence, PSL and PS induced persistent luminescence

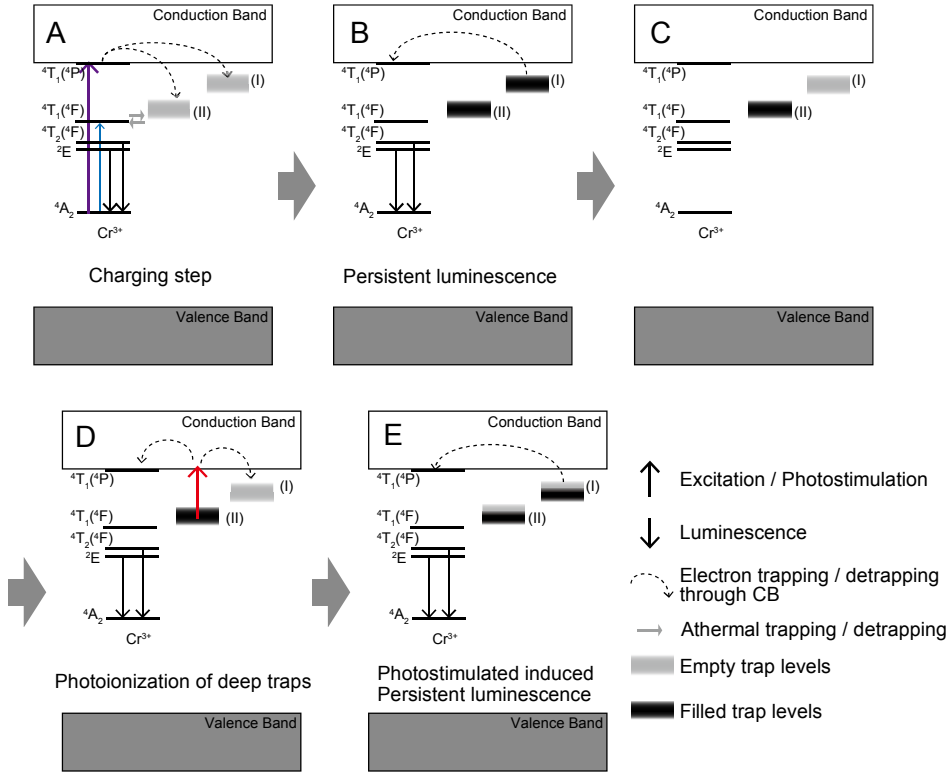

Fig. 7. Explanation of persistent luminescence, photostimulated luminescence and photostimulation induced persistent luminescence in the YAG*G*:Cr^{3+}. Energy level diagram corresponds to Cr^{3+} states before releasing an electron and after capturing an electron (B, C, D, E). The red arrow in Part (D) represents 625 nm photostimulation.

Figure 7 shows schemes of the persistent luminescence, PSL and photostimulation induced persistent luminescence mechanisms in the YAG*G*:Cr^{3+} based on electron trapping model.

#256933 Received 8 Jan 2016; revised 7 Mar 2016; accepted 8 Mar 2016; published 31 Mar 2016

Energy scale is estimated according to [10, 19]. In Fig. 7(a), an efficient electron trapping to both trap (I) and (II) occurs through the conduction band under UV excitation at 254 nm. On the other hand, notice that under blue ($^4A_2 \rightarrow {}^4T_2$) excitation, inefficient partial trap filling occurs, only in the deeper part of trap (II). After stopping UV excitation light, persistent luminescence appears mainly due to the detrapping of traps (I) and the following recombination occurs through the conduction band (Fig. 7(b)). After several hours, no more electrons are trapped by the shallower traps (I) (Fig. 7(c)). Then for example upon 625 nm red photostimulation (Red arrow in Fig. 7(d)), electrons are released from deep traps (II) and resulting in PSL. At the same time, partial retrapping occurs from trap (II) to trap (I) (Fig. 7(d)). After stopping photostimulation, persistent luminescence is observed again as shown in Fig. 7(e) and Fig. 8.

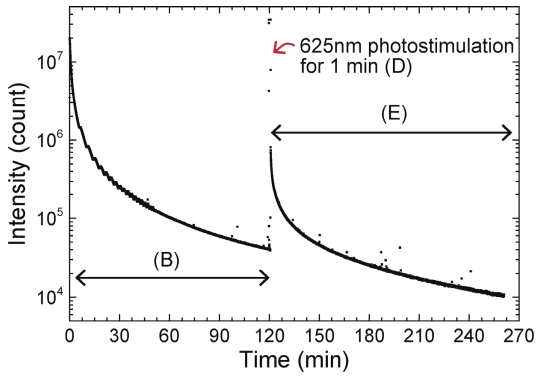

Fig. 8. Persistent luminescence after 5 min UV excitation and following photostimulated persistent luminescence after 1 min red photostimulation.

4. Conclusion

Light storage ability of YAG*G*:Cr^{3+} deep red persistent phosphor was investigated by temperature dependence of PL spectra and TSL glow curves under different excitation wavelength, waiting time, temperature and photostimulation wavelength. The integrated PL intensity of Cr^{3+} luminescence ($^2E \rightarrow {}^4A_2$ plus $^4T_2 \rightarrow {}^4A_2$ transitions) suffers very little from temperature quenching up to 600 K. In the TSL glow curve after UV excitation, there are two kinds of TSL bands peaking at 311 K and 394 K, which have shallowest trap depth of 0.38 eV and 0.76 eV respectively. The effect of photostimulation was also investigated. 1.27 eV and 1.53 eV photons can release shallower traps as well as 1.98 eV photon can release the shallower traps and a part of the deeper traps, which result in PSL. After releasing electrons from the shallower traps, the reactivation of the shallower traps by red to near-infrared photostimulation was observed. This result reveals that photostimulation induced persistent luminescence can be possible in the YAG*G*:Cr^{3+}. This phenomenon can provide a tool for long-term *in vivo* imaging.

Acknowledgments

This work was financially supported by a Grant-in-Aid for Scientific Research from JSPS Fellows (No.26-40075) and by French ANR-PEPSI.

#256933 Received 8 Jan 2016; revised 7 Mar 2016; accepted 8 Mar 2016; published 31 Mar 2016